JAAS

PAPER

View Article Online
View Journal | View Issue

Cite this: *J. Anal. At. Spectrom.*, 2019, **34**, 1800

Determination of Zr isotopic ratios in zircons using laser-ablation multiple-collector inductively coupled-plasma mass-spectrometry†

Wen Zhang,[a] Zaicong Wang,[a] Frédéric Moynier,[b] Edward Inglis,[b] Shengyu Tian,[b] Ming Li,[a] Yongsheng Liu[a] and Zhaochu Hu*[a]

Received 3rd June 2019
Accepted 1st July 2019

DOI: 10.1039/c9ja00192a

rsc.li/jaas

This study presents the first high precision method to analyze stable Zr isotope ratios in zircons using laser ablation multiple collector inductively coupled plasma mass spectrometry (LA-MC-ICP-MS). Interference problems for *in situ* Zr isotope analysis were investigated in detail. The polyatomic interferences of $^{89}Y^{1}H^{+}$ and doubly charged ion interference of $^{180}Hf^{++}$ did not influence the Zr isotope analysis. The addition of 8 ml min^{-1} nitrogen to the central gas flow in LA-MC-ICP-MS was found to increase the sensitivity of Zr by a factor of 1.95. The analysis mode of small laser spot sizes (16–32 μm) and low laser frequency (1 Hz) combined with a signal-smoothing device was used. Compared to that without the signal-smoothing device, the obtained analytical precision was improved by about 60.6 times by using the signal-smoothing device at the low laser frequency (1 Hz). The accuracy of the *in situ* method is validated by comparing the data to those of a well-established double spike solution method. Data for six international zircon standards and six additional natural zircons are given. The data are reported as standard delta notation as the permil deviation of the $^{94}Zr/^{90}Zr$ ($\delta^{94/90}Zr_{GJ\text{-}1}$) and $^{96}Zr/^{90}Zr$ ($\delta^{96/90}Zr_{GJ\text{-}1}$) ratios relative to the GJ-1 zircon standard. Typical intermediate precisions for $\delta^{94/90}Zr_{GJ\text{-}1}$ and $\delta^{96/90}Zr_{GJ\text{-}1}$ were 0.11 and 0.18‰ (2SD, standard deviation). The $\delta^{94/90}Zr_{GJ\text{-}1}$ values for the four zircon reference materials (91500, Plešovice, Penglai and Mud Tank) determined by LA-MC-ICP-MS were in good agreement with those of double spiked solution measurements, confirming the accuracy of the *in situ* method. The zircon reference material FC1 showed the largest stable isotope fractionation of 4.93‰ for $\delta^{94/90}Zr_{GJ\text{-}1}$. One natural zircon (08KQ02-1) with a complex history showed a significant $\delta^{94/90}Zr_{GJ\text{-}1}$ isotope variation in the single grain. These results suggest that Zr isotopes are a potentially powerful geochemical tracer and that high spatial-resolution, *in situ* determination like by the LA-MC-ICP-MS method in this study is rather important to identify Zr isotope variation in single zircon grains.

1. Introduction

The ^{92}Nb–^{92}Zr extinct radioactive decay system and nucleosynthetic anomalies of ^{96}Zr have received much attention within the field of Zr isotope geochemistry.[1–8] Only recently have natural, mass dependent stable isotope variations been explored,[9,10] which is at odds given the key role zircon has played in unraveling major geological problems.[11–14]

Recently there has been an increasing interest in studying mass-dependent isotope variations of Zr in geological samples utilizing a double-spike solution MC-ICP-MS.[9,10] These studies have shown that igneous rocks display significant stable isotope variations of $\delta^{94/90}Zr_{IPGP\text{-}Zr}$, the permil deviation of the $^{94}Zr/^{90}Zr$ ratio relative to the IPGP-Zr standard. These isotopic fractionations were observed within a suite of co-genetic lavas from the Hekla volcano in Iceland spanning bulk compositional variations from basalt to rhyolite, amounting to a differentiation suite. They demonstrated that the most evolved samples were isotopically heavier, up to 0.57‰, when compared to primitive basalts. This isotopic variation was interpreted to reflect the preferential sequestering of light Zr isotopes into the 8-fold coordinated sites of zircon relative to 6-fold coordinated basaltic melts.[15] Therefore, Zr stable isotopes have the potential to trace magmatic processes, such as igneous differentiation and the evolution and growth of continental crust.[9,10]

Early Zr isotope measurements were performed using thermal ionization mass spectrometry (TIMS),[16,17] but because Zr has a high first ionization potential (660 KJ mol^{-1}), its ionization yield is low on TIMS, as such the use of multiple collector

[a]*State Key Laboratory of Geological Processes and Mineral Resources, School of Earth Sciences, China University of Geosciences, Wuhan 430074, China. E-mail: zchu@vip.sina.com; Fax: +86 27 67885096; Tel: +86 27 61055600*

[b]*Institut de Physique du Globe de Paris, University of Paris, Université Paris Diderot, CNRS, 1 rue Jussieu, 75238 Paris Cedex 05, France*

† Electronic supplementary information (ESI) available: (A) The image data of natural zircons. (B) The analytical results of trace elements in eleven zircons using LA-ICP-MS. (C) The signal intensity of the potential interference elements. See DOI: 10.1039/c9ja00192a

inductively coupled plasma mass spectrometry (MC-ICP-MS) is better suited owing to the ionization potential of plasma source instruments. Furthermore, MC-ICP-MS offers the potential for higher rates of sample throughput relative to TIMS as well as the possibility to perform *in situ* measurement when coupled to a laser ablation system. MC-ICP-MS studies of non-mass dependent variations of Zr isotopes use a pair of Zr isotopes ($^{91}Zr/^{90}Zr$ or $^{94}Zr/^{90}Zr$) to correct the instrumental mass fractionation.[2,5–8,18–21] This approach is very precise (<10 ppm, 2SD (standard deviation) for most normalized isotope ratios) but the internal standardization method also corrects for the natural mass-dependent isotope fractionation. Recently a state of the art approach to study natural mass-dependent isotopic variations based on a double-spike MC-ICP-MS method has been developed.[9] This method utilizes a ^{91}Zr–^{96}Zr double spike to correct for any fractionations imparted during sample processing and mass spectrometry. The data are normalized to a pure Zr standard solution (Zr-IPGP) and reported in standard delta notation. Using such a method the $\delta^{94/90}Zr_{IPGP\text{-}Zr}$ values for six rock reference materials were reported with an external precision of ~44 ppm (2SD). This pioneering study opens up the field of Zr stable isotope geochemistry to trace natural mass-dependent Zr isotope variations related to geological processes.

It is suggested that zircon is a key phase in fractionating Zr isotope ratios within magmatic systems.[10] Furthermore zircon constitutes a geochemical data repository of unparalleled quality owing to its resistance to later thermal events, a high closure temperature for radiogenic isotope systems and its widespread occurrence as an accessory mineral in many rocks. Because of these features zircon has been widely used to determine the age and the thermal history of rocks and decipher the evolution of the Earth's crust and mantle.[13,22,23] *In situ* micro analysis techniques have been used to determine the UPb dating age and Hf–O–Si (also other isotopes and trace elements) isotope ratios in zircons by using laser ablation-(MC)-ICP-MS[24–27] and secondary ion mass spectroscopy (SIMS).[28–31] However, no studies have used such micro analysis techniques for the direct, *in situ*, analysis of mass-dependent stable Zr isotope variations.[18–20]

Here, we report the first *in situ* stable Zr isotope analysis method in natural zircons using LA-MC-ICP-MS. We present the optimal analytical parameters, such as the investigation of potential interferences, the addition of N_2 and the laser ablation mode, to obtain high precision and accurate Zr isotope ratios. The Zr isotopic compositions of six zircon reference materials and six additional zircon grains are reported. To validate the accuracy, the Zr isotopic composition of reference zircons by LA-MC-ICP-MS is compared to results obtained by the wet chemistry double spike method and we also report the isotopic shift between the GJ-1 zircon standard (used in this study as a reference) and the IPGP-Zr standard used in wet chemistry studies.

2. Experimental

2.1 Instrumentation

2.1.1 LA-MC-ICP-MS. *In situ* Zr isotope analyses were performed on a Neptune *Plus* MC-ICP-MS instrument (Thermo Fisher Scientific, Bremen, Germany), which was connected to a 193 nm excimer ArF laser ablation system (GeoLas HD, Coherent Inc., Göttingen, Germany), at the State Key Laboratory of Geological Processes and Mineral Resources, China University of Geosciences in Wuhan. The Faraday collector configuration of the mass spectrometer was composed of an array from L4 to H2 to monitor $^{89}Y^+$, $^{90}Zr^+$, $^{91}Zr^+$, $^{92}Zr^+$, $^{94}Zr^+$, $^{95}Mo^+$, and $^{96}Zr^+$ (Table 1). The laser ablation was conducted under a helium atmosphere in the ablation cell with a volume of *ca.* 40 cm^3, an inlet nozzle (i.d. <0.5 mm) and a wide outlet (i.d. 1.5 mm), while argon was mixed into the sample-out line downstream from the ablation chamber prior to entering the torch of the mass spectrometer. To decrease the tau effect (essentially a delay in the response of the resistors), a new signal-smoothing device was used downstream from the sample cell, which approximately eliminated the short-term variability of the signal.[32] Details of the instrumental operating conditions and measurement parameters are summarized in Table 1.

2.2 Samples

Six international zircon reference materials (GJ-1, 91500, Plešovice, Penglai, Mud Tank and FC1) were used in this study. GJ-1 was used for tuning and as the bracketing standard for isotope measurements. These zircons are widely used as reference materials for the microanalysis of U–Pb, Hf and O isotopes. Additionally, six natural zircon megacrysts were sampled from Brazil, Burma, Malawi, Norway, Pakistan and Tanzania. Photographs of the natural zircon grains analysed here are shown in Fig. S1 (ESI A†). All samples were mounted in 25 mm epoxy discs and ground with grit paper to expose the interior of the material. The sample surfaces were then polished using a diamond abrasive and were subsequently cleaned with a soap

Table 1 Summary of the operating parameters for MC-ICP-MS and the 193 nm excimer laser ablation system

MC-ICP-MS (NEPTUNE Plus)							
Cup-configuration	L4	L3	L2	L1	C	H1	H2
	$^{89}Y^+$	$^{90}Zr^+$	$^{91}Zr^+$	$^{92}Zr^+$	$^{94}Zr^+$	$^{95}Mo^+$	$^{96}Zr^+$
RF power	1250 W						
Cool gas flow	16.0 L min^{-1}						
Auxiliary gas flow	0.80 L min^{-1}						
Argon make-up gas flow	~0.70 L min^{-1}						
Helium carrier gas flow	~0.60 L min^{-1}						
Nitrogen gas flow	0, 4, 8 ml min^{-1}						
Interface cones	X skimmer cone + Jet sample cone						
Mass resolution	Low						
Block number	1						
Cycles of each block	120						
Integration time (s)	0.524 s						
Laser ablation system (GeoLas Pro)							
Laser type	ArF excimer laser						
Wavelength	193 nm						
Pulse length	15 ns						
Energy density	~10 J cm^{-2}						
Ablation mode	Single spot						
Spot size	16–32 μm						
Laser frequency	1–2 Hz						

solution, distilled water and ethanol in an ultrasonic bath prior to analysis.

2.3 Analytical method

2.3.1 Laser ablation analysis. For *in situ* Zr isotope measurements a high sensitivity X-skimmer cone and Jet-sample cone were mounted in the Neptune Plus interface. The mass spectrometer was operated in the low mass resolution mode. A small amount of N_2 (8 ml min^{-1}) was added to the carrier gas flow behind the signal-smoothing device through a simple Y connector. A zircon reference material, GJ-1, was used to optimize the instrumental parameters, including the He and Ar gas flow rates, the torch position, the RF power setting, and the source lens settings. This allowed us to achieve the suitable sensitivity and the optimum peak shape.

The routine data acquisition consisted of one block of 120 cycles (0.524 second integration time per cycle): the first 30 cycles were measured in order to determine the background, while the remaining 90 cycles were measured for the sample. The laser was run with an output energy (constant energy mode) of 60 mJ, producing a power density on the sample of approximately ~8 J cm^{-2}. Because zircons comprise ~50 wt% Zr, a large Zr signal intensity can be obtained with a small ablated spot size. The Zr isotope analysis in this study was completed with laser spot sizes of 16–32 μm and a low laser frequency of 1 Hz. Using the low ablation frequency is important to reduce the risk of isotope fractionation by the increased depth/diameter ratio of the ablation crater with time, especially for the small ablated spot size. Under these operating conditions a signal intensity of ~15 V at the mass of ^{90}Zr for GJ-1 was achieved. Background intensities were <0.001 V at the mass of ^{90}Zr. To avoid the possible position effect in the Zr isotope ratio analysis, all samples in this study were tightly placed with the reference material GJ-1. A detailed summary of the instrument operating parameters for the laser system and MC-ICP-MS is listed in Table 1.

Because isotope measurements by laser ablation do not benefit from the advantages of matrix purification by ion exchange chromatography, it is not possible to purify the samples from possible matrix interferences. As such it is of paramount importance to assess the source of potential interferences that may be encountered during analysis. The major interferences for Zr masses are listed in Table 2, including the isobaric interferences, doubly charged ion interferences and polyatomic interferences. However, trace element measurement of zircon grains by LA-ICP-MS demonstrates that most of the interfering elements (Ti, V, Cr, Mn, Fe, Ni, Ge, As, Se, Mo, Ta and W) occur at very low concentrations, often below the detection limit of ICP-MS (given the average ppb level) (Table S1, ESI B†). Therefore, the interferences of these elements on the Zr isotope masses are considered to be negligible. In addition, the signal intensities of other interference elements (Kr, Ru, Os, and Pt) were independently collected using the mass scan mode in MC-ICP-MS (Fig. S2, ESI C†), when a zircon reference material Mud Tank was measured under common instrumental conditions. The signal intensity of ^{90}Zr in Mud Tank was ~27.7 V, while the signal intensities of Kr, Ru, Os, and Pt cannot be distinguished from the blank signals. Therefore, the interferences of Kr, Ru, Os and Pt can also be negligible.

Both Y and Hf, which are commonly enriched in zircons, could potentially cause interferences with Zr masses. The analytical results in Table S1† show that the concentrations of Y and Hf in the eleven zircons vary over a wide range, such as 104–4213 μg g^{-1} and 5415–11 874 μg g^{-1}, respectively. The polyatomic interference of $^{89}Y^1H^+$ can be resolved from $^{90}Zr^+$ at a resolving power of ~10 000. Although the Neptune *Plus* instrument provides a maximum resolving power ($m/\Delta m$, 5%

Table 2 List of the potential interferences on Zr isotopes in zircons by LA-MC-ICP-MS. Numbers in brackets are the isotope abundance (%)

Isotopes	Isobaric interferences	Doubly charged ion interferences	Polyatomic interferences
^{90}Zr(51.452)		**$^{180}Hf^{++}$(35.080)** $^{180}W^{++}$(0.120) $^{180}Ta^{++}$(0.012)	$^{50}Ti(5.185)^{40}Ar^+(99.604)$ $^{50}Cr(4.345)^{40}Ar^+(99.604)$ $^{50}V(0.250)^{40}Ar^+(99.604)$ $^{74}Ge(36.523)^{16}O^+(99.76)$ $^{74}Se(0.863)^{16}O^+(99.76)$ **$^{89}Y(100)^1H^+(99.99)$**
^{91}Zr(11.223)		$^{182}W^{++}$(26.499)	$^{55}Mn(100)^{36}Ar^+(0.334)$ $^{51}V(99.750)^{40}Ar^+(99.604)$ $^{75}As(100)^{16}O^+(99.762)$
^{92}Zr(17.146)	**$^{92}Mo^+$(14.649)**	$^{184}W^{++}$(30.642) $^{184}Os^{++}$(0.019)	$^{56}Fe(91.754)^{36}Ar^+(0.334)$ $^{52}Cr(83.790)^{40}Ar^+(99.604)$ $^{76}Ge(7.745)^{16}O^+(99.76)$ $^{76}Se(9.220)^{16}O^+(99.76)$
^{94}Zr(17.380)	**$^{94}Mo^+$(9.187)**	$^{188}Os^{++}$(13.243)	$^{58}Ni(68.077)^{36}Ar^+(0.334)$ $^{54}Fe(5.845)^{40}Ar^+(99.604)$ $^{54}Cr(2.365)^{40}Ar^+(99.604)$ $^{78}Se(23.685)^{16}O^+(99.76)$ $^{78}Kr(0.355)^{16}O^+(99.76)$
^{96}Zr(2.799)	**$^{96}Mo^+$(16.673)** $^{96}Ru^+$(5.542)	$^{192}Pt^{++}$(0.782) $^{192}Os^{++}$(40.781)	$^{56}Fe(91.7540)^{40}Ar^+(99.604)$ $^{80}Kr(2.286)^{16}O^+(99.76)$ $^{80}Se(49.813)^{16}O^+(99.76)$

and 95%) of 10 000, the ion intensity of Zr would be compromised in the high-resolution mode. A detailed study was implemented by analyzing a Mud Tank zircon grain and a xenotime (YPO_4) under the same instrumental conditions. Then the signal intensities were collected in the mass range from 88.5 to 93.5 (Fig. 1). The signal intensity of $^{89}Y^1H^+$ can be calculated after blank and ^{90}Zr correction using the ^{92}Zr signal and the natural $^{90}Zr/^{92}Zr$ of 3.001. A very low yield of $^{89}Y^1H^+$ was obtained (1.6×10^{-6}), which was attributed to the addition of N_2. It has been previously shown that the addition of N_2 can suppress polyatomic interferences (oxides and hydrides).[33–35] Therefore, we believe that the interferences of Y do not influence the Zr isotope masses measured in our method.

The doubly charged ion interference of $^{180}Hf^{++}$ on mass 90 can be assessed by monitoring the signal intensity of $^{179}Hf^{++}$ at mass 89.5. Fig. 2 shows the signal intensities of $^{179}Hf^+$, $^{180}Hf^+$ and $^{179}Hf^{++}$, when Mud Tank was ablated. Mud Tank has a high concentration of Hf (~9291 μg g^{-1}), but the signal intensities of $^{179}Hf^+$ and $^{180}Hf^+$ were only 0.14 V and 0.37 V, respectively. No signal intensity of $^{179}Hf^{++}$ was observed. This can be attributed to the high second ionization energy of Hf (14.93 eV), producing the low doubly charged ion of Hf under the specific conditions employed during Zr isotope measurements. Therefore, the doubly charged ion interference of $^{180}Hf^{++}$ on mass 90 can be considered non-existent.

In summary, no interference correction was implemented in this study, but the $^{89}Y^+$ and $^{95}Mo^+$ signals were monitored. The deviation between the LA measured results and solution values from MC-ICP-MS in zircon reference materials and a three-isotope plot ($\delta^{94/90}Zr_{GJ\text{-}1}$ *vs.* $\delta^{94/91}Zr_{GJ\text{-}1}$) was used to assess the presence of other potential interferences. The assessment results will be discussed in the following section.

The standard-sample bracketing technique (SSB) was applied for correcting the mass fractionation and instrument drift. The analytical sequence proceeded by bracketing two samples with the measurement of two standards. The average isotope ratio of the standards was calculated and used as a reference for the sample. The relative difference in the isotope ratios between the sample and standard was calculated using the δ notation, as shown in eqn (1) (using $^{94}Zr/^{90}Zr$ as an example), and was expressed in parts per thousand.

$$\delta^{94/90}Zr = \left[\frac{\left(\frac{^{94}Zr}{^{90}Zr}\right)_{sample}}{\left(\frac{^{94}Zr}{^{90}Zr}\right)_{standard}} - 1\right] \times 1000 \quad (1)$$

The zircon reference material GJ-1 was employed as the matrix-matching standard. All δ values were reported relative to GJ-1. Three Zr isotope ratios were calculated in this study, including $^{94}Zr/^{90}Zr$, $^{94}Zr/^{91}Zr$ and $^{96}Zr/^{90}Zr$. However, $^{94}Zr/^{91}Zr$ used to evaluate the interference problem in the three-isotope plot ($\delta^{94/90}Zr_{GJ\text{-}1}$ *vs.* $\delta^{94/91}Zr_{GJ\text{-}1}$). In the following, we only report the results of $^{94}Zr/^{90}Zr$ and $^{96}Zr/^{90}Zr$.

Data were reduced in the following order and based upon user-selected background and sample integration intervals. The average background was first subtracted from the raw Zr signals. During each run, the ratios of the ion beams at $^{94}Zr/^{90}Zr$, $^{94}Zr/^{91}Zr$ and $^{96}Zr/^{90}Zr$ were calculated. The ratios were averaged into a single measured value after exclusion of replicates that deviated >2SD from the average. The final Zr isotope ratios were calculated by correcting for instrumental mass fractionation using the external standard GJ-1. The within-run precision for one single spot analysis was calculated by the combination of the SE (standard error) from samples and standards using the following equation:

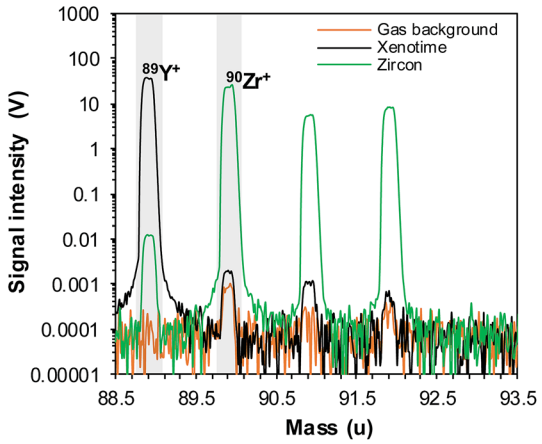

Fig. 1 The signal intensities from mass 88.5 to 93.5 when a zircon Mud Tank and a xenotime (YPO_4) were analyzed under the same instrumental conditions. The signal intensities in gas background are shown.

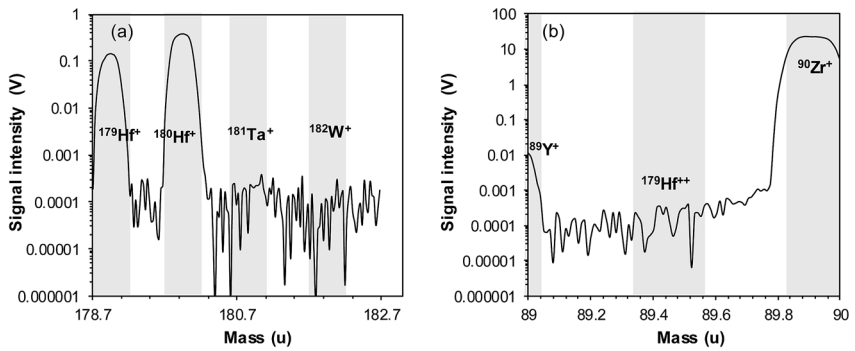

Fig. 2 The signal intensities of $^{179}Hf^+$ (a), $^{180}Hf^+$ (a) and $^{179}Hf^{++}$ (b) when a zircon Mud Tank was analyzed.

$$2SE = 2 \times \sqrt{(SE_{sample})^2 + (SE_{standard\text{-}1})^2 + (SE_{standard\text{-}2})^2} \quad (2)$$

where SE_{sample} is the standard error of the Zr isotope ratio of the sample, and $SE_{standard\text{-}1}$ and $SE_{standard\text{-}2}$ are the standard error of the Zr isotope ratio of the former and the latter bracketing standard, respectively. All data reduction for the LA-MC-ICP-MS analysis of Zr isotope ratios was conducted using "Iso-Compass" in-house software, which is new in-house software specifically designed for isotope ratio analysis (please send an email to the author for free software).

2.3.2 Solution-MC-ICP-MS analysis. The $\delta^{94/90}Zr_{IPGP\text{-}Zr}$ for four zircon reference materials (GJ-1, 91500, Penglai and Mud Tank) investigated in this study was determined using solution-MC-ICP-MS with a double spike method relative to the IPGP-Zr standard. These measurements were conducted at the Institut de Physique du Globe de Paris, France. Zirconium isotope measurements were performed using the method described by Tian *et al.* (submitted) and Inglis *et al.*[9,36] In addition, the solution value of $\delta^{94/90}Zr_{IPGP\text{-}Zr}$ for the zircon Plešovice has been previously reported by Inglis *et al.*[9]

The zircon GJ-1 was used as an external standard for the LA study and in order to compare LA and solution measurements. All δ values were converted to GJ-1 using the $\delta^{94/90}Zr_{IPGP\text{-}Zr}$ of GJ-1 $= -0.012 \pm 0.042$ (2SD). The values obtained for the solution measurements are listed in Table 3.

2.3.3 *In situ* element concentration analysis in zircons by LA-ICP-MS. For the LA-ICP-MS elemental measurements a 193 nm ArF excimer laser ablation system (GeoLas HD, Coherent Inc., Göttingen, Germany) coupled to an Agilent 7500a quadrupole ICP-MS (ICP-MS) instrument (Agilent Technologies, Tokyo, Japan), was used for the determination of major and trace element concentrations in zircons. Detailed operating conditions for the laser ablation system and the ICP-MS instrument and data reduction were the same as described by Hu *et al.*[34] and Liu *et al.*,[37] and are listed in ESI B.†

Table 3 Zr isotopic compositions of eleven zircons measured by LA-MC-ICP-MS and solution-MC-ICP-MS

	LA-MC-ICP-MS[a]					Solution MC-ICP-MS[b]	
Number		$\delta^{94/90}Zr_{GJ\text{-}1}$	2SD	$\delta^{96/90}Zr_{GJ\text{-}1}$	2SD	$\delta^{94/90}Zr_{GJ\text{-}1}$	2SD
Zircon reference materials							
91500	52	0.00	0.11	0.00	0.17	−0.01	0.06
Plešovice	38	0.14	0.10	0.21	0.19	0.12	0.06
Penglai	36	−0.14	0.12	−0.22	0.20	−0.11	0.06
Mud Tank	40	0.04	0.15	0.05	0.22	0.09	0.05
FC1	29	0.27	1.90	0.42	2.85		
Nature zircons							
Zr-Bra	11	0.03	0.15	0.10	0.20		
Zr-Kuf	12	−0.03	0.15	−0.03	0.21		
Zr-Mala	19	−0.16	0.12	−0.24	0.19		
Zr-Bur	12	0.08	0.16	0.11	0.24		
Zr-Paki	38	0.24	0.11	0.37	0.20		
Zr-Tan	13	0.10	0.13	0.13	0.18		

[a] GJ-1 was used as the external standard for all samples. The $\delta^{94/90}Zr$ of GJ-1 relative to the IPGP-Zr standard ($\delta^{94/90}Zr_{IPGP\text{-}Zr}$) is -0.01 ± 0.04. [b] Data from Tian *et al.* (submitted)[36] except Plešovice which is from Inglis *et al.* (2018).[9]

3. Results and discussion

3.1 Effect of the addition of N_2 on signal intensity

The addition of N_2 in LA-MC-ICP-MS has been reported to improve the signal intensity of Hf and Nd.[25,38] Since Zr and Hf have similar first ionization energies (6.64 eV and 6.83 eV, respectively), the addition of N_2 into ICP should also increase the sensitivity of Zr. N_2 has a thermal conductivity, which is higher than that of argon by a factor of 32 at 7000 K.[39] Therefore, the addition of N_2 in the ICP would improve the plasma temperature in the center channel, resulting in sensitivity enhancements for the elements with high first ionization energy or evaporation enthalpy. Fig. 3 shows the signal intensity of ^{90}Zr in the zircon reference material GJ-1 at a spot size of 32 μm and a repetition rate of 1 Hz as a function of makeup gas flow rates in both the normal and the nitrogen modes (4 and 8 ml min^{-1}). The signal intensities of ^{90}Zr increased with the addition of N_2. The maximum signal enhancements with the addition of nitrogen at 4 ml min^{-1} and 8 ml min^{-1} were 1.66 and 1.95 times for Zr.

3.2 Effect of the signal-smoothing device on the low laser frequency mode

Many zircons have complex growth zones or small grain sizes. Therefore, increasing the spatial resolution of analytical methods is important for *in situ* zircon analysis. On the other hand, it has been known that continuous pulsing of the laser introduces a time-dependent isotopic fractionation with increasing crater depth,[40,41] especially at small spot sizes. In this study, a low laser frequency mode (1–2 Hz) was used to minimize the potential isotope fractionation effect and control the signal intensity of Zr. Fig. 4 shows the variation of the signal

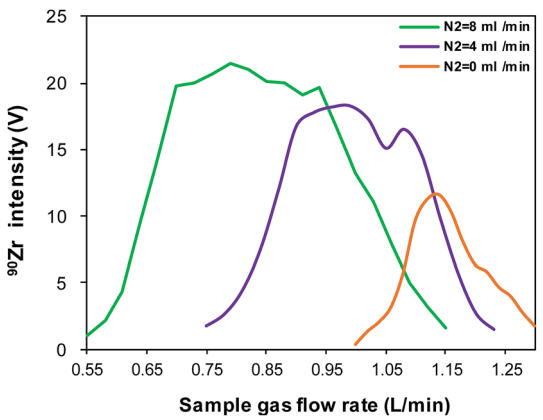

Fig. 3 The signal intensities of ^{90}Zr from a zircon reference material GJ-1 at a spot of 32 μm and repetition rate of 1 Hz as a function of makeup gas flow rates in both the normal and the nitrogen (4 to 8 ml min^{-1}) modes.

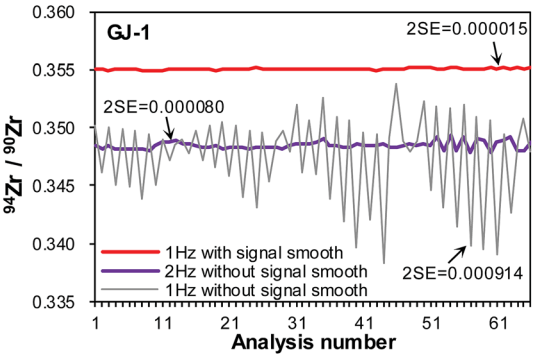

Fig. 4 Time-resolved variation of the $^{94}Zr/^{90}Zr$ ratio in zircon GJ-1 using 1–2 Hz laser ablation with and without the signal-smoothing device.

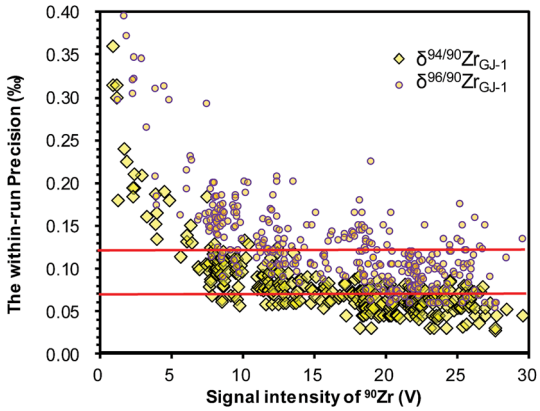

Fig. 5 The relationship between ^{90}Zr signal intensity and the within-run precision of $\delta^{94/90}Zr_{GJ\text{-}1}$ and $\delta^{96/90}Zr_{GJ\text{-}1}$ for *in situ* Zr isotope analysis of zircon reference materials at different laser spot sizes (10–32 μm) and different laser frequencies of 1–2 Hz.

ratio of $^{94}Zr/^{90}Zr$ with time during laser ablation of zircon GJ-1 at a spot size of 32 μm and a laser frequency of 1–2 Hz using the standard ablation cell. When the ablation frequency was at 1 Hz, the isotope ratio of $^{94}Zr/^{90}Zr$ exhibited a regular and screw-like variation pattern, which significantly influenced the Zr isotope analytical precision (2SE = 0.000914). Increasing the laser frequency to 2 Hz can improve this phenomenon (2SE = 0.000080), but it still falls outside of the range otherwise attainable. A signal-smoothing device, which has been previously reported by Hu *et al.*,[32] was used to eliminate the screw-like pattern in the low laser frequency mode. When compared to data obtained without using the signal-smoothing device, the analytical precision of $^{94}Zr/^{90}Zr$ (2SE = 0.000015) is improved by about 60.6 times when running at a laser frequency of 1 Hz (Fig. 4).

The use of small spot sizes and low laser frequency combined with a signal-smoothing device not only showed a significant improvement in the analytical precision but also provided a good spatial resolution in the vertical direction. In our method, the depth of ablation pits within zircon grains is ~3.5 μm (1 Hz, 50 pulses) or 7 μm (1 Hz, 100 pulses), which is beneficial for revealing the Zr isotope information in complex zircons through the analysis of layer by layer.

3.3 Intensity *vs.* within-run precision

It is well known that analytical precision is strongly dependent on the signal intensity. Fig. 5 shows the relationship between the ^{90}Zr signal intensity (the average signal of the single spot analysis) and the within-run precisions of $\delta^{94/90}Zr_{GJ\text{-}1}$ (2SE) on individual Zr isotope ratio measurements when using the signal-smoothing device. The measurement precision for $\delta^{94/90}Zr_{GJ\text{-}1}$ significantly improved as the ^{90}Zr signal intensity increased from 0.10 to 15 V, followed by more gradual enhancements at higher signal intensities (>15 V). Generally, when the $^{90}Zr^+$ signal intensity is higher than 15 V, the within-run precision of $\delta^{94/90}Zr_{GJ\text{-}1}$ was lower than 0.07‰ (2SE). A worse within-run precision of $\delta^{96/90}Zr_{GJ\text{-}1}$ was observed (0.12‰, 2SE) due to the lower abundance of ^{96}Zr (Fig. 5). However, the high signal intensity would be harmful for the life of the Faraday cup. We can choose the lower signal intensity (10–15 V) by using a smaller spot size of 16 μm and a slower repetition rate of 1 Hz. In this case, the within-run precisions of $\delta^{94/90}Zr_{GJ\text{-}1}$ and $\delta^{96/90}Zr_{GJ\text{-}1}$ are normally 0.08‰ (2SE) and 0.013‰ (2SE), respectively, which satisfy the analytical requirement.

3.4 Results for zircon reference materials and natural zircons

Based on these studies, the addition of 8 ml min^{-1} N_2 combined with the signal-smoothing device was used for Zr isotopic ratio measurements in six zircon reference materials, including GJ-1, 91500, Plešovice, Penglai, Mud Tank and FC1. First, we established the optimum intermediate precision of our method by analyzing two GJ-1 fragments in two individual analytical sessions. Each test lasted approximately one hour and consisted of ~30 single spot analyses. One of the GJ-1 fragments was used as an external standard and another as an unknown sample. The intermediate precision was expressed as the two times standard deviation (2SD). Fig. 6 shows the analytical results of $\delta^{94/90}Zr_{GJ\text{-}1}$ and $\delta^{96/90}Zr_{GJ\text{-}1}$ in the unknown sample (GJ-1). The measured values in two individual analytical sequences were 0.00 ± 0.09‰ and 0.01 ± 0.09‰ for $\delta^{94/90}Zr_{GJ\text{-}1}$, and 0.00 ± 0.12‰ and 0.01 ± 0.14‰ for $\delta^{96/90}Zr_{GJ\text{-}1}$. These values represented the upper limit of precision for our method in the repeated analyses over the course of one hour.

The $\delta^{94/90}Zr_{GJ\text{-}1}$ and $\delta^{96/90}Zr_{GJ\text{-}1}$ values for five other zircon reference materials (91500, Plešovice, Penglai, Mud Tank and FC1) obtained from the repeated measurements over four months are compiled in Fig. 7 and Table 3. The obtained results of zircon 91500 ($\delta^{94/90}Zr_{GJ\text{-}1} = 0.00 \pm 0.11$‰, $\delta^{96/90}Zr_{GJ\text{-}1} = 0.00 \pm 0.17$‰; 2SD, $n = 52$), Plešovice ($\delta^{94/90}Zr_{GJ\text{-}1} = 0.14 \pm 0.10$‰, $\delta^{96/90}Zr_{GJ\text{-}1} = 0.21 \pm 0.19$‰; 2SD, $n = 38$), Panglai ($\delta^{94/90}Zr_{GJ\text{-}1} = -0.14 \pm 0.12$‰, $\delta^{96/90}Zr_{GJ\text{-}1} = -0.22 \pm 0.20$‰; 2SD, $n = 36$) and Mud Tank ($\delta^{94/90}Zr_{GJ\text{-}1} = 0.04 \pm 0.15$‰, $\delta^{96/90}Zr_{GJ\text{-}1} = 0.05 \pm 0.22$‰; 2SD, $n = 40$) agree with the values obtained by solution MC-ICP-MS within the uncertainty, confirming the accuracy of the presented analytical protocol.[9,36] The validated analytical method was used to analyse six natural zircon grains

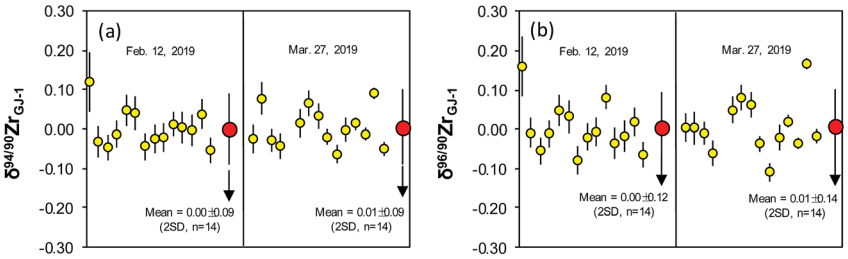

Fig. 6 $\delta^{94/90}Zr_{GJ-1}$ (a) and $\delta^{96/90}Zr_{GJ-1}$ (b) values for repeat analysis of the GJ-1 zircon grain from two individual analytical sessions.

(Table 2). Repeat analyses for these zircons at a laser spot size of 32 μm and a repetition rate of 1 Hz yielded intermediate precisions of 0.11–0.16‰ (2SD) for $\delta^{94/90}Zr_{GJ-1}$ and 0.18–0.24‰ (2SD) for $\delta^{96/90}Zr_{GJ-1}$. Combining data from these ten zircons (four zircon reference materials and six zircon grains), significant isotopic variations of $\delta^{94/90}Zr_{GJ-1}$ and $\delta^{96/90}Zr_{GJ-1}$ were observed from −0.16 to 0.24‰ and from −0.24 to 0.37‰, respectively (Table 2).

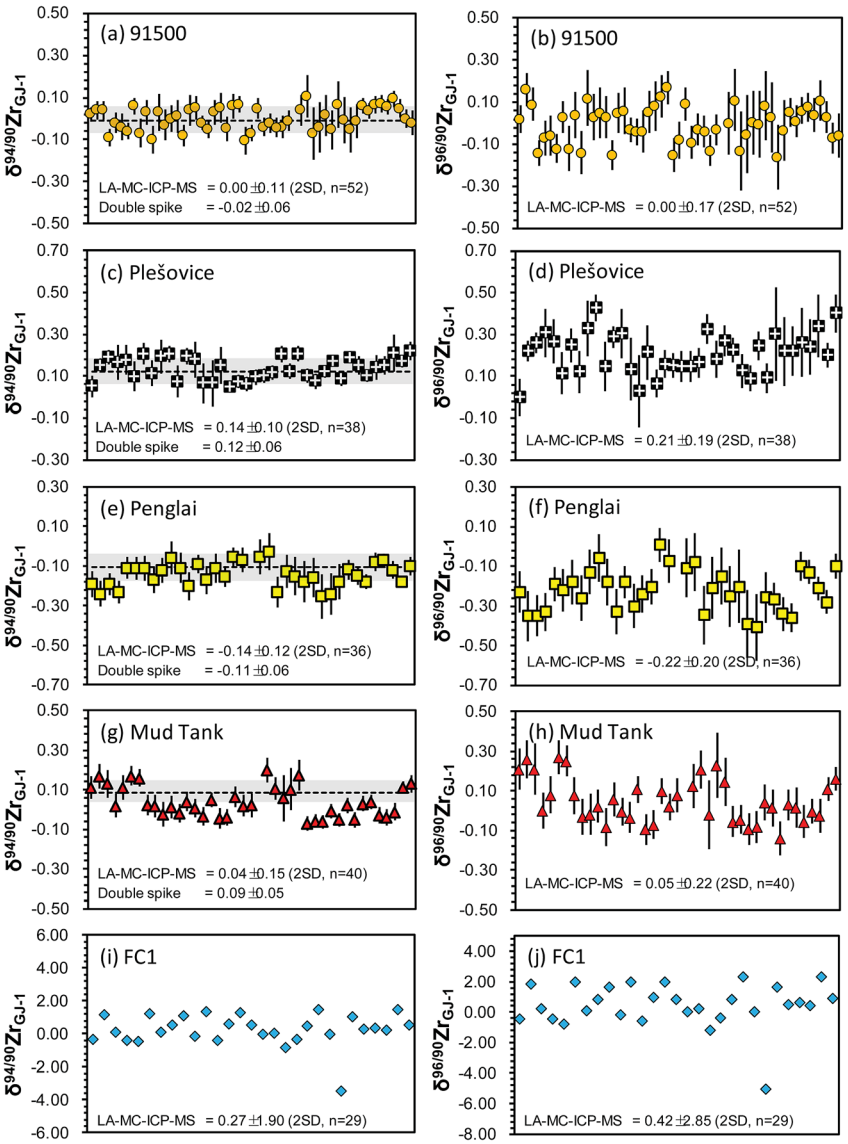

Fig. 7 A compilation of $\delta^{94/90}Zr_{GJ-1}$ and $\delta^{96/90}Zr_{GJ-1}$ in five zircon reference materials obtained from repeated measurements in different analytical sessions over four months. Error bars represent the within-run precision. The average values for the double spike measurements are plotted as black broken lines. The grey area represents the error range of the double spike values. Within each plot, the data are presented in chronological order.

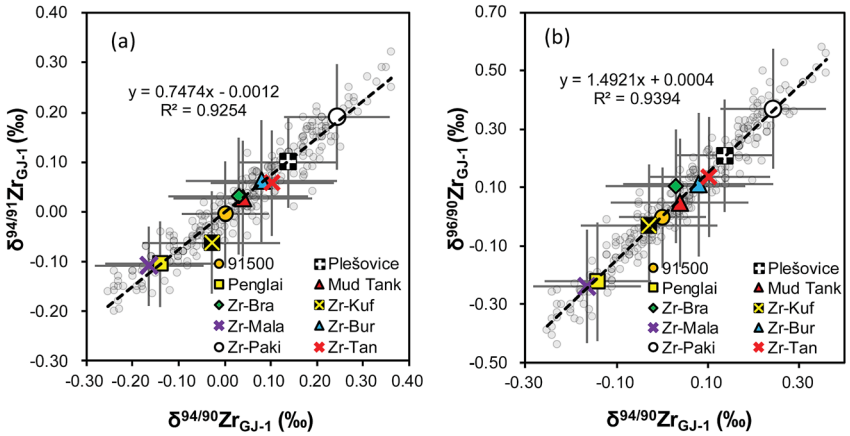

Fig. 8 A three-isotope plot ($\delta^{94/90}Zr_{GJ\text{-}1}$ *vs.* $\delta^{94/91}Zr_{GJ\text{-}1}$) of the Zr isotopic compositions in ten zircons obtained using LA-MC-ICP-MS (a). A multi-isotope plot ($\delta^{94/90}Zr_{GJ\text{-}1}$ *vs.* $\delta^{96/90}Zr_{GJ\text{-}1}$) of the Zr isotopic compositions in ten zircons obtained using LA-MC-ICP-MS (b). The grey dots represent all measured data. The coloured symbols represent the average values of each sample with the uncertainty (2SD).

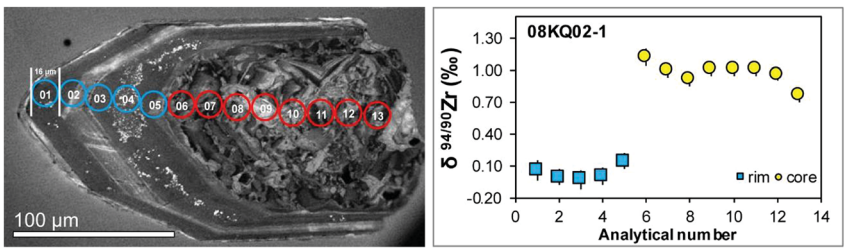

Fig. 9 One natural zircon (08KQ02-1) with a core-rim structure in the CL image was measured at a laser spot size of 16 μm and a repetition rate of 1 Hz.

The analytical results in zircon reference material FC1 showed a significant heterogeneity of Zr isotope compositions. The average values of $\delta^{94/90}Zr_{GJ\text{-}1}$ and $\delta^{96/90}Zr_{GJ\text{-}1}$ in FC1 were 0.27 ± 1.90‰ (2SD) and 0.42 ± 2.85‰ (2SD), respectively (Fig. 7 and Table 3). The variation of $\delta^{94/90}Zr_{GJ\text{-}1}$ in FC1 is up to 4.93‰, which is the largest stable isotope fractionation we have found in natural zircons so far. FC1 is derived from the Anorthositic Series of the Duluth Complex in north-eastern Minnesota.[42] The concordant U–Pb age data and the homogeneous Hf isotope composition in FC1 have been reported by Frei and Gerdes (2009) and Kemp *et al.* (2009).[43,44] But the reason for such significant Zr isotope variation in FC1 is still unclear. It is apparent that the FC-1 zircons are not suitable as reference materials for *in situ* Zr isotope analysis.

A multi-isotope plot is commonly used for identifying mass independent fractionation, isobaric interference and analytical artifacts. All measured data of the Zr isotopic compositions in ten zircon samples and their average values are plotted in two multi-isotope plots ($\delta^{94/90}Zr_{GJ\text{-}1}$ *vs.* $\delta^{94/91}Zr_{GJ\text{-}1}$; $\delta^{94/90}Zr_{GJ\text{-}1}$ *vs.* $\delta^{96/90}Zr_{GJ\text{-}1}$) (Fig. 8). The analytical results of FC1 are not compiled in Fig. 8. The slopes of regression lines in two plots were calculated for all measured data. ^{91}Zr could experience different interference relative to ^{90}Zr. The slope of 0.7474 for $\delta^{94/90}Zr_{GJ\text{-}1}$ *vs.* $\delta^{94/91}Zr_{GJ\text{-}1}$ was in agreement with the theoretical kinetic fraction value of 0.7458, confirming that the analytical results of $\delta^{94/90}Zr_{GJ\text{-}1}$ and $\delta^{94/91}Zr_{GJ\text{-}1}$ are not influenced by any interferences. In addition, the slope of 1.4921 in $\delta^{94/90}Zr_{GJ\text{-}1}$ *vs.* $\delta^{96/90}Zr_{GJ\text{-}1}$ was also in agreement with the theoretical kinetic fraction value of 1.4844, further indicating the reliability of the proposed method.

In order to display the advantage of the new Zr isotope analytical method using LA-MC-ICP-MS further, one natural zircon (08KQ02-1) with a core-rim structure in the CL image was measured at a laser spot size of 16 μm and a repetition rate of 1 Hz (Fig. 9). The spot analyses located from the core to the rim and showed significant stable isotope variation. Zircon 08KQ02-1 has high Zr isotope compositions in the core (average $\delta^{94/90}Zr_{GJ\text{-}1}$ of 0.98 ± 0.19‰) and sharply decreased toward the rim (average $\delta^{94/90}Zr_{GJ\text{-}1}$ of 0.04 ± 0.13‰) (Fig. 9). The exact cause of this phenomenon remains unclear, and more studies are needed combined with meticulous petrology and mineralogy. Nevertheless, this case demonstrates that *in situ* Zr isotope analysis using LA-MC-ICP-MS can provide a new perspective for deciphering the complex mineral crystallization history of some zircons.

4. Conclusion

This study presents the first protocol to measure *in situ* high-precision Zr isotope compositions of zircons by LA-MC-ICP-MS. Interference problems for *in situ* Zr isotope analysis were

investigated in detail. Our data results indicate that there is no interference in the proposed LA-MC-ICP-MS method, and this method can be used to obtain precise and accurate data. In order to investigate the Zr isotope composition of complexly zoned zircons or small particle sizes, the improvement of the spatial resolution is important. The analysis mode of small spot sizes and low laser frequency combined with a signal-smoothing device is recommended. The results presented here demonstrate that the signal-smoothing device was necessary for the accurate and precise determination of Zr isotopic ratios when analysed under the low laser frequency conditions. The low frequency (1 Hz) and the small number of ablation pulses (~50 pulses) in this study produced a shallow ablation pit (3.5–7.0 μm), which provide an opportunity for achieving high spatial resolution Zr isotope compositions in the vertical direction. A typical analytical precision of $\delta^{94/90}Zr_{GJ\text{-}1}$ and $\delta^{96/90}Zr_{GJ\text{-}1}$ for natural zircon grains, achieved by the present LA-MC-ICP-MS technique, was 0.11 and 0.18‰ (2SD) respectively. The $\delta^{94/90}Zr_{GJ\text{-}1}$ values for the four zircon reference materials (91500, Plešovice, Penglai and Mud Tank) determined by LA-MC-ICP-MS were in good agreement with values for the same samples obtained by solution double spike MC-ICP-MS methods, thus confirming the accuracy of the proposed method. However, the zircon reference material FC1 had a significant variation of Zr isotope compositions among different grains and showed the largest stable isotope fractionation of 4.93‰ for $\delta^{94/90}Zr_{GJ\text{-}1}$ reported so far. Additionally, one natural zircon (08KQ02-1) with a complex history displayed a significant intra-grain Zr isotope heterogeneity. These results demonstrate that significant Zr isotopic variations occur within natural zircons, and are easily identified using the proposed LA-MC-ICP-MS method.

Conflicts of interest

There are no conflicts to declare.

Acknowledgements

This research is supported by the Chinese State Key Research and Development Program (2016YFE0203000), the National Natural Science Foundation of China (Grants 41603002, 41730211 and 41725013) and the most special fund from the State Key Laboratory of Geological Processes and Mineral Resources, China University of Geosciences (MSFGPMR04 and MSFGPMR08).

References

1 J. F. Minster and C. J. Allègre, *Geochim. Cosmochim. Acta*, 1982, **46**, 565–573.
2 C. Münker, S. Weyer, K. Mezger, M. Rehkämper, F. Wombacher and A. Bischoff, *Science*, 2000, **289**, 1538–1542.
3 C. Sanloup, J. Blichert-Toft, P. Télouk, P. Gillet and F. Albarède, *Earth Planet. Sci. Lett.*, 2000, **184**, 75–81.
4 M. Schönbächler, M. Rehkämper, A. N. Halliday, D.-C. Lee, M. Bourot-Denise, B. Zanda, B. Hattendorf and D. Günther, *Science*, 2002, **295**, 1705–1708.
5 M. Schönbächler, D. C. Lee, M. Rehkämper, A. N. Halliday, M. A. Fehr, B. Hattendorf and D. Günther, *Earth Planet. Sci. Lett.*, 2003, **216**, 467–481.
6 W. Akram, M. Schönbächler, S. Bisterzo and R. Gallino, *Geochim. Cosmochim. Acta*, 2015, **165**, 484–500.
7 T. Iizuka, Y. J. Lai, W. Akram, Y. Amelin and M. Schönbächler, *Earth Planet. Sci. Lett.*, 2016, **439**, 172–181.
8 W. Akram and M. Schönbächler, *Earth Planet. Sci. Lett.*, 2016, **449**, 302–310.
9 E. C. Inglis, J. B. Creech, Z. Deng and F. Moynier, *Chem. Geol.*, 2018, **493**, 544–552.
10 E. C. Inglis, F. Moynier, J. Creech, Z. Deng, J. M. D. Day, F.-Z. Teng, M. Bizzarro, M. Jackson and P. Savage, *Geochim. Cosmochim. Acta*, 2019, **250**, 311–323.
11 E. B. Watson and T. M. Harrison, *Earth Planet. Sci. Lett.*, 1983, **64**, 295–304.
12 A. I. S. Kemp, C. J. Hawkesworth, G. L. Foster, B. A. Paterson, J. D. Woodhead, J. M. Hergt, C. M. Gray and M. J. Whitehouse, *Science*, 2007, **315**, 980–983.
13 B. Dhuime, C. J. Hawkesworth, P. A. Cawood and C. D. Storey, *Science*, 2012, **335**, 1334–1336.
14 Y. B. Wu and Y. F. Zheng, *Chin. Sci. Bull.*, 2004, **49**, 1554–1569.
15 F. Farges, C. W. Ponader and G. E. Brown, *Geochim. Cosmochim. Acta*, 1991, **55**, 1563–1574.
16 S. K. Sahoo and A. Masuda, *Chem. Geol.*, 1997, **141**, 117–126.
17 M. B. Greiter, V. Höllriegl and U. Oeh, *Int. J. Mass Spectrom.*, 2011, **304**, 1–8.
18 T. Hirata and T. Yamaguchi, *J. Anal. At. Spectrom.*, 1999, **14**, 1455–1459.
19 Q. Z. Yin, S. B. Jacobsen, W. F. McDonough, I. Horn, M. I. Petaev and J. Zipfel, *Astrophys. J.*, 2000, **536**, L49–L53.
20 T. Hirata, *Chem. Geol.*, 2001, **176**, 323–342.
21 M. Schönbächler, M. Rehkämper, D. C. Lee and A. N. Halliday, *Analyst*, 2004, **129**, 32–37.
22 C. J. Hawkesworth and A. I. S. Kemp, *Chem. Geol.*, 2006, **226**, 144–162.
23 T. M. Harrison, A. K. Schmitt, M. T. McCulloch and O. M. Lovera, *Earth Planet. Sci. Lett.*, 2008, **268**, 476–486.
24 H. L. Yuan, S. Gao, M. N. Dai, C. L. Zong, D. Günther, G. H. Fontaine, X. M. Liu and C. R. Diwu, *Chem. Geol.*, 2008, **247**, 100–118.
25 Z. C. Hu, Y. S. Liu, S. Gao, W. G. Liu, W. Zhang, X. R. Tong, L. Lin, K. Q. Zong, M. Li, H. h. Chen, L. Zhou and L. Yang, *J. Anal. At. Spectrom.*, 2012, **27**, 1391–1399.
26 S. E. Jackson, N. J. Pearson, W. L. Griffin and E. A. Belousova, *Chem. Geol.*, 2004, **211**, 47–69.
27 Y. S. Liu, Z. C. Hu, K. Q. Zong, C. G. Gao, S. Gao, J. Xu and H. H. Chen, *Chin. Sci. Bull.*, 2010, **55**, 1535–1546.
28 M. F. Zhou, D. P. Yan, A. K. Kennedy, Y. Q. Li and J. Ding, *Earth Planet. Sci. Lett.*, 2002, **196**, 51–67.
29 J. W. Valley, *Rev. Mineral. Geochem.*, 2003, **53**, 343–385.
30 X. H. Li, W. X. Li, Z. X. Li, C. H. Lo, J. Wang, M. F. Ye and Y. H. Yang, *Precambrian Res.*, 2009, **174**, 117–128.

31 D. Trail, P. Boehnke, P. S. Savage, M. C. Liu, M. L. Miller and I. Bindeman, *Proc. Natl. Acad. Sci. U. S. A.*, 2018, **115**, 10287–10292.
32 Z. C. Hu, W. Zhang, Y. S. Liu, S. Gao, M. Li, K. Q. Zong, H. H. Chen and S. H. Hu, *Anal. Chem.*, 2015, **87**, 1152–1157.
33 J. L. Fu, Z. C. Hu, W. Zhang, L. Yang, Y. S. Liu, M. Li, K. Q. Zong, S. Gao and S. H. Hu, *Anal. Chim. Acta*, 2016, **911**, 14–26.
34 Z. C. Hu, S. Gao, Y. S. Liu, S. H. Hu, H. H. Chen and H. L. Yuan, *J. Anal. At. Spectrom.*, 2008, **23**, 1093–1101.
35 G. L. Scheffler and D. Pozebon, *Anal. Methods*, 2014, **6**, 6170–6182.
36 S. Y. Tian, E. Inglis, J. Creech, W. Zhang, Z. C. Wang, Z. C. Hu, Y. S. Liu and F. Moynier, *J. Anal. At. Spectrom.*, 2019, submitted to.
37 Y. S. Liu, Z. C. Hu, S. Gao, D. Günther, J. Xu, C. G. Gao and H. H. Chen, *Chem. Geol.*, 2008, **257**, 34–43.
38 L. Xu, Z. C. Hu, W. Zhang, L. Yang, Y. S. Liu, S. Gao, T. Luo and S. H. Hu, *J. Anal. At. Spectrom.*, 2015, **30**, 232–244.
39 S. F. Durrant, *Fresenius' J. Anal. Chem.*, 1994, **349**, 768–771.
40 S. M. Eggins, L. P. J. Kinsley and J. M. G. Shelley, *Appl. Surf. Sci.*, 1998, **127–129**, 278–286.
41 I. Horn, R. L. Rudnick and W. F. McDonough, *Chem. Geol.*, 2000, **164**, 281–301.
42 J. B. Paces and J. D. Miller, *J. Geophys. Res.*, 1993, **98**, 13997–14013.
43 D. Frei and A. Gerdes, *Chem. Geol.*, 2009, **261**, 261–270.
44 A. I. S. Kemp, G. L. Foster, A. Scherstén, M. J. Whitehouse, J. Darling and C. Storey, *Chem. Geol.*, 2009, **261**, 244–260.